Chemical Physics 428 (2014) 137–143

Contents lists available at ScienceDirect

Chemical Physics

journal homepage: www.elsevier.com/locate/chemphys

Spectroscopic properties of $ErAl_3(BO_3)_4$ single crystal

A.V. Malakhovskii *, T.V. Kutsak, A.L. Sukhachev, A.S. Aleksandrovsky, A.S. Krylov, I.A. Gudim, M.S. Molokeev

L.V. Kirensky Institute of Physics, Siberian Branch, Russian Academy of Sciences, 660036 Krasnoyarsk, Russian Federation

ARTICLE INFO

Article history:
Received 21 August 2013
In final form 6 November 2013
Available online 20 November 2013

Keywords:
Rare earth compounds
Er^{3+}
Spectroscopic properties
Judd–Ofelt analysis
Luminescence

ABSTRACT

Single crystal of $ErAl_3(BO_3)_4$ was grown and its structure was studied. Polarized absorption spectra of $ErAl_3(BO_3)_4$ single crystal were measured in the spectral range 1670–330 nm (6000–30000 cm^{-1}). The Judd–Ofelt spectroscopic parameters have been determined: $\Omega_2 = 4.87 \times 10^{-20}$ cm^2, $\Omega_4 = 2.49 \times 10^{-20}$ cm^2, $\Omega_6 = 2.72 \times 10^{-20}$ cm^2. These parameters have been used to calculate the radiative transition probabilities, the multiplet luminescence branching ratios and the fluorescence life times of the manifolds. The luminescence spectra due to transitions $^2H_{11/2} \rightarrow {}^4I_{15/2}$ (526 nm), $^4S_{3/2} \rightarrow {}^4I_{15/2}$ (548 nm), $^4F_{9/2} \rightarrow {}^4I_{15/2}$ (662 nm), $^2H_{11/2} \rightarrow {}^4I_{13/2} + {}^4I_{9/2} \rightarrow {}^4I_{15/2}$ (800 nm) and $^4S_{3/2} \rightarrow {}^4I_{13/2}$ (855 nm) were recorded in α, σ and π polarizations. The most intensive luminescence belonged to $^4S_{3/2} \rightarrow {}^4I_{15/2}$ transition (548 nm).

1. Introduction

Crystalline lasers attract heightened attention of researches due to their numerous applications in various quantum electronics and optical devices. Er^{3+} is widely used active ion in solid state lasers. In particular, laser generation was obtained in $YAl_3(BO_3)_4$ crystal with admixture of Er^{3+} ion [1–3]. Spectroscopic properties of Er^{3+} ion were studied in many materials (e.g. [4–8]) and, in particular, in $Er:YAl_3(BO_3)_4$ crystal [9–13]. Borates $RM_3(BO_3)_4$ (R–Y or rare earth (RE) metal, M–Al, Ga, Cr, Fe, Sc) have huntite-like structure with the trigonal space group *R32* (D_3^7). Rare earth ions are situated in a D_3 crystal field without center of inversion. Therefore, crystals of this type can be used also as nonlinear active media [14,15]. Erbium-containing crystals are attractive as materials demonstrating up-conversion luminescence due to energy transfer between excited ions of the same kind [16]. (See also [17,18]). As far as we know, spectroscopic properties of the stoichiometric $ErAl_3(BO_3)_4$ crystal were not studied yet. However, just crystals with large concentration of the active ion can be suitable for solid state microchip lasers [19–21], which are necessary for a number of technological applications. This paper presents polarized absorption spectra and a systematic characterization of the spectroscopic parameters of the $ErAl_3(BO_3)_4$ crystal, which are essential for understanding its laser gain capability. The parity forbidden *f–f* transitions absorption spectra are treated with the help of the Judd–Ofelt (J–O) theory, and spectroscopic parameters obtained are compared with those of some other erbium containing compounds. Luminescence on some transitions was also recorded.

2. Experimental details

Single crystals of $ErAl_3(BO_3)_4$ were grown at small overcooling on seeds from the flux 90% mass ($Bi_2Mo_3O_{12} + 2B_2O_3 + 0{,}5Li_2MoO_4$) + 10% mass $ErAl_3(BO_3)_4$. This flux has saturation temperature $T_{sat} = 960$ °C. Details of the growth procedure have been described in Ref. [22]. Earlier the same crystal was grown from another flux [23]. As grown-up crystals had the size of $5 \times 5 \times 7$ mm^3. Bi and Mo occurrence and their influence on some optical properties of Yb doped alumoborate were estimated in Ref. [24]. $ErAl_3(BO_3)_4$ single crystal has strongly anisotropic magnetic properties [25].

The X-ray single crystal data from $ErAl_3(BO_3)_4$ were measured by SMART APEX II diffractometer (Mo K_α, $\lambda = 0.7106$ Å) at room temperature. The matrix of orientation and cell parameters were calculated and refined by 1702 reflections. The main information about crystal data, data collection and refinement are reported in Table 1. The X-ray data from $ErAl_3(BO_3)_4$ crystal were measured for the exposure time of 10 s on each frame. Each new frame was obtained by crystal rotation along ω-axis by 0.5° at the fixed φ angle. The ω value was increased from 0 to 182°. The 364 frames were measured at each fixed φ equal to 0, 120, and 240°. After that, the program APEXII from Bruker integrated the intensities of reflections. Space group *R32* was defined by analysis of extinction rules and intensity statistics obtained from all reflections. Multiscan absorption correction

* Corresponding author. Tel.: +7 391 2498617; fax: +7 391 2438923.
E-mail address: malakha@iph.krasn.ru (A.V. Malakhovskii).

0301-0104/$ - see front matter © 2013 Elsevier B.V. All rights reserved.
http://dx.doi.org/10.1016/j.chemphys.2013.11.008

Table 1
Crystallographic data and main parameters of processing and refinement of $ErAl_3(BO_3)_4$.

Crystal data	
Chemical formula	$ErAl_3(BO_3)_4$
M_r	483.44
space group, Z	*R32*, 3
a, (Å)	9.2833(7)
c, (Å)	7.2234(6)
V, (Å^3)	539.11(7)
D_x, Mg/m^3	4.467
μ, mm^{-1}	12.133
size	0.3 × 0.2 × 0.2
Data collection	
wavelength	MoK_α, λ = 0.7106 Å
measured reflections	1707
independent reflections	329
reflections with $I > 2\sigma(I)$	329
absorption correction	multiscan
R_{int}	0.0277
$2\theta_{max}$ (°)	59.48
h	−12 → 12
k	−12 → 12
l	−9 → 9
Refinement	
$R[F^2 > 2\ (F^2)]$	0.0104
$wR(F^2)$	0.0237
S	0.929
weight	$w = 1/\sigma^2(F_o^2)$
Flack parameter [26]	−0.056(11)
number parameters/restraints	20/0
$(\Delta/\sigma)_{max}$	<0.001
$\Delta\rho_{max}$, e/Å^3	0.77
$\Delta\rho_{min}$, e/Å^3	−0.59
extinction correction coefficient (SHELX97)	0.0249(9)

of reflection intensities was performed by APEXII software. Then, the intensities of equivalent reflections were averaged. The structure of $ErAl_3(BO_3)_4$ was solved by direct methods using the SHELXS program [27]. The coordinates of all atoms were determined. The structure refinement was carried out by least-squares minimization in SHELXL97 [28]. Thermal parameters of Er and Al were refined anisotropically. Further details of the crystal structure may be obtained from Fachinformationszentrum Karlsruhe, 76344 Eggenstein-Leopoldshafen, Germany (fax: +49 7247 808 666; E-mail: crystdata@fiz-karlsruhe.de; http://www.fiz-karlsruhe.de/request_for_deposited_data.html on quoting the deposition number CSD-426751).

As mentioned above, the crystal belongs to trigonal symmetry class with the space group *R*32, and its lattice constants (Table 1) are very close to cell parameters from [29]: $a = 9.285(3)$ Å and $c = 7.222(3)$. The unit cell contains three formula units. Trivalent rare-earth (RE) ions occupy positions of only one type. They are located at the center of trigonal prisms made up of six crystallographically equivalent oxygen ions. The triangles formed by the oxygen ions in the neighboring basal planes are not superimposed on each other but are twisted by a certain angle. Owing to this distortion, the symmetry D_{3h} of the ideal prism is reduced to the symmetry D_3 [30]. The AlO_6 octahedrons share edges in such a way that they form helicoidal chains, which run parallel to the C_3 axis and are mutually independent. All Al ions occupy C_2-symmetry positions in the crystal.

The absorption spectra were measured by the two beam technique, using an automated spectrophotometer designed on the basis of the diffraction monochromator MDR-2. They were obtained with the light propagating normally to the C_3 axis of the crystal for the light electric vector $\vec{E}$ parallel (π spectrum) and perpendicular (σ spectrum) to the C_3 axis, and for the light propagating along the C_3 axis (α spectrum). Optical slit with (spectral resolution) was 0.4 nm in the region of 300–600 nm and 0.8 nm in the region of 600–1100 nm. Spectra of luminescence at room temperature were obtained on the Horiba Jobin Ivon T6400 Raman spectrophotometer with the excitation by argon laser at the wavelength 488 nm (20490 cm^{-1}). Applicability of the T64000 spectrophotometer for high quality luminescent measurements was recently described in Ref. [31]. The radiation 20 mW of argon laser was focused onto the crystal to the diameter of 10 micron.

3. Results and discussion

Absorption spectra of the $ErAl_3(BO_3)_4$ crystal for π and σ polarizations at room temperature were measured in the spectral range 1670–330 nm (6000–30000 cm^{-1}) and are shown in Figs. 1 and 2 (decimal absorption coefficients). Identification of *f*–*f* absorption bands was made according to Kaminskii [32]. The absorption spectra measured in the σ- and α-polarizations coincide within the limit of the experimental error. This implies that the absorption mainly occurs through the electric dipole mechanism. The absorption spectra reveal substantial dichroism. Majority of absorption bands are more intensive in σ-polarization.

Intensities of absorption bands in π- and σ-polarizations were found as integrals $I = \int \frac{\alpha(E)}{C} dE$ over the bands, where C is the molar concentration in mol/l and E is the quantum energy in cm^{-1} (Table 2). The transition intensities were averaged over the polarizations according to common relation for uniaxial anisotropic crystals: $I = (2I_\sigma + I_\pi)/3$. Following to Ref. [33], oscillator strengths of transitions $I \to F$ between J multiplets were calculated by the formula:

$$f_{IF} = 4.318 \times 10^{-9} \frac{3n}{(n)^2 + 2} I_{IF}. \quad (1)$$

Refractive index n of alumoborates slightly depends on rare earth ion. Basing on data obtained in Refs. [34,35], it is possible to show that average refractive index, taking into account wavelength dependence both refractive index and birefringence, over the entire spectral range under investigation is equal to 1.75 with accuracy of ±3%. This error results in ±0.7% error of oscillator strengths calculation according to (1). The determined oscillator strengths of the transitions are given in Table 2. The transition strength is defined as: $s_{IF} = \frac{1}{e^2}\sum_{if}|\vec{D}_{if}|^2$, where $i \in I$, $f \in F$ and $\vec{D}_{if}$ is the matrix element of the electric dipole moment. The transition strength and the oscillator strength are related by the expression [36].

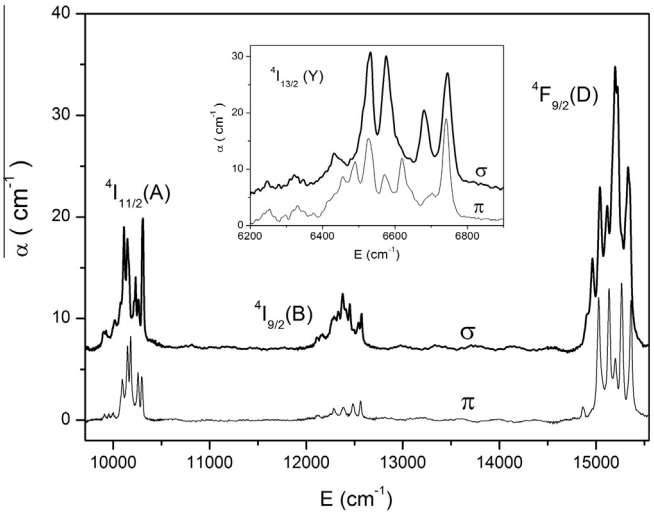

Fig. 1. Polarized (π and σ) absorption spectra of $ErAl_3(BO_3)_4$ single crystal in infra red spectral range at room temperature. Terminal states of transitions from the ground $^4I_{15/2}$ state are indicated.

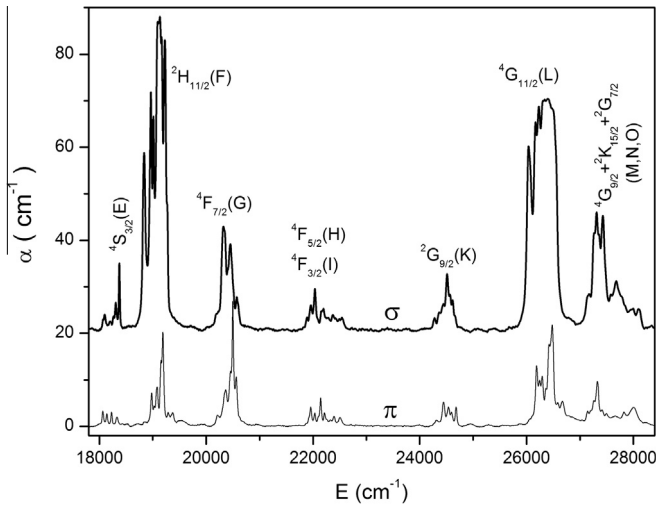

Fig. 2. Polarized (π and σ) absorption spectra of $ErAl_3(BO_3)_4$ single crystal in visible spectral range at room temperature. Terminal states of transitions from the ground $^4I_{15/2}$ state are indicated.

$$s_{IF} = \frac{3hg_I}{8\pi^2 mck_{IF}} f_{IF}, \tag{2}$$

where g_I is the degree of degeneracy of the initial state and k_{IF} is the average wave number of the absorption band. Experimentally found strengths of the *f–f* transitions are given in Table 2.

In the framework of the J–O theory, the strength of an *f–f* transition in an ion in the non centrosymmetrical crystal field is described by the relationship [37–39].

$$s_{IF} = \sum_{\lambda} \Omega_\lambda \Gamma^2_\lambda(I,F). \tag{3}$$

Coefficients $\Gamma^2_\lambda(I,F) = \langle I\|U^{(\lambda)}\|F\rangle^2$ are calculated theoretically and are considered to be independent of crystal structure. They are given in Ref. [32]. The index λ for the *f–f* transitions takes three values: 2, 4, and 6. The transitions under consideration in a free Er^{3+} ion are forbidden in the electric dipole approximation not only by the parity, but some of them are forbidden by the total momentum in accordance with the selection rule $\Delta J = 0, \pm 1$. According to the Judd–Ofelt theory [39], when transitions are allowed by the parity selection rule due to the odd components of the crystal field, they can occur at $\Delta J \leqslant \lambda$ ($\lambda = 2$, 4, and 6 as mentioned above). Therefore, within this approximation, all considered *f–f* transitions in the Er^{3+} ion are allowed. Transitions $^4I_{15/2} \rightarrow {}^2H_{11/2}$ and $^4G_{11/2}$ are the most intensive one (see Fig. 2 and Table 2). Indeed, they are the only transitions with large values of coefficient Γ^2_2 (Table 2) and, consequently, Ω_2 parameter is the actual one. This means that 1-st and 3-d spherical harmonics t ($t = \lambda \pm 1$[39]) in the expansion of the crystal field take part in the allowance of the mentioned transitions by parity, while only higher harmonics are active in the allowance of the rest of transitions.

Eq. (3) can be written in the vector form:

$$\vec{s} = A\vec{\Omega}. \tag{4}$$

Here $\vec{s}$ – is a q-dimensional vector, consisting of the measured strengths of the transition groups; q – is the number of the considered groups of transitions; $\vec{\Omega}$ – is the three-dimensional vector of parameters Ω_λ; A – is the $3 \times q$-dimentional matrix of the $\Gamma^2_\lambda(I,F)$ coefficients. The vector $\vec{\Omega}$ that minimizes the sum of the squares of the deviations between the measured and theoretical transition strengths is given by the matrix equation [40]

$$\vec{\Omega} = \left(A^T A\right)^{-1} A^T \vec{s}, \tag{5}$$

where A^T – is the transposed matrix. All groups of the measured transitions were used for calculation, and obtained parameters Ω_λ are shown in Table 3. The J–O parameters of some other erbium containing crystals are also presented in Table 3. Transition strengths calculated from Eq. (3) with the found parameters Ω_λ are given in Table 2. The relative root mean square error of the theoretical description of the transition strengths is defined by equation

$$\delta = \left[\frac{q\sum \Delta s^2}{(q-p)\sum s^2}\right]^{1/2}. \tag{6}$$

Here values s are the measured transition strengths, Δs are the differences between the measured and calculated transition strengths, p is the number of the determined parameters, being equal to 3 in our case. With the help of (6) and Table 2 we obtain $\delta \approx 17\%$.

The equal population of all crystal field split components of the ground state is one of the main postulates of the J–O theory, but this condition is usually not fulfilled for rare earth ions. In particular, the total CF splitting of Er^{3+} ground state in the $Er:YAl_3(BO3)_4$ crystal is 316 cm^{-1} (455 K) [9]. Therefore, the mentioned postulate is not satisfied at room temperature, and the integral transition intensities can change with the temperature. If they change proportionally to each other, then it is possible to consider that the effective Judd–Ofelt parameters change correspondingly. Temperature dependencies of integral intensities of some absorption bands in $ErAl_3(BO3)_4$ are presented in Fig. 3. One can see that the integral intensities change with temperature substantially not identically. This already principally violates the mentioned postulate and is

Table 2
Parameters of transitions: Γ^2_λ – coefficients in the J–O Eq. (3), k_{IF} – average wave numbers of absorption bands, I_{IF} – integral intensities of absorption bands, f_{IF} – oscillator strengths of transitions, s_{IF} – strengths of transitions.

Label	Excited state	Γ^2_2	Γ^2_4	Γ^2_6	k_{IF} (cm^{-1})	I_{IF} (cm^{-2} mol^{-1}l)		f_{IF} (10^{-7})	s_{IF} (10^{-20} cm^2)	
						π	σ		Exp.	Calc.
Y	$^4I_{13/2}$	0.0195	0.1173	1.4316	6500	352	504	20.3	4.57	4.278
A	$^4I_{11/2}$	0.0282	0.0003	0.3953	10190	99	216	7.92	1.15	1.212
B	$^4I_{9/2}$	0	0.1732	0.0099	12400	46	128	4.50	0.54	0.458
D	$^4F_{9/2}$	0	0.5354	0.4619	15180	292	678	24.6	2.39	2.588
E	$^4S_{3/2}$	0	0	0.2211	18220	66	122	4.63	0.374	0.601
F	$^2H_{11/2}$	0.7125	0.4123	0.0925	19120	338	2288	73.3	5.65	4.748
G	$^4F_{7/2}$	0	0.1468	0.6266	20450	367	569	22.5	1.62	2.068
H + I	$^4F_{5/2}$ + $^4F_{3/2}$	0	0	0.3505	22200	152	251	9.76	0.65	0.953
K	$^2G_{9/2}$	0	0.0190	0.2255	24530	130	250	9.4	0.57	0.66
L	$^4G_{11/2}$	0.9181	0.5261	0.1171	26400	671	2892	96.3	5.39	6.1
M + N+O	$^4G_{9/2}$ + $^2K_{15/2}$+$^2G_{7/2}$	0.0219	0.263	0.3154	27550	376	1136	39.5	2.12	1.618

Table 3
J–O parameters of Er^{3+} ion in some laser crystals.

Crystal	$\Omega_2 \times 10^{-20}$ cm^2	$\Omega_4 \times 10^{-20}$ cm^2	$\Omega_6 \times 10^{-20}$ cm^2	Reference
$ErAl_3(BO_3)_4$	4.87	2.49	2.72	This work
$Er:YAl_3(BO_3)_4$	8.38	1.61	1.50	[12]
$Er:YAl_3(BO_3)_4$	6.54	1.89	1.81	[41]
Er:YAG	0.74	0.33	1.02	[7]
$Er:YVO_4$	13.45	2.33	1.67	[6]
$Er:YAlO_3$	0.95	0.58	0.55	[4]
$Er:LiNbO_3$	7.29	2.24	1.27	[5]

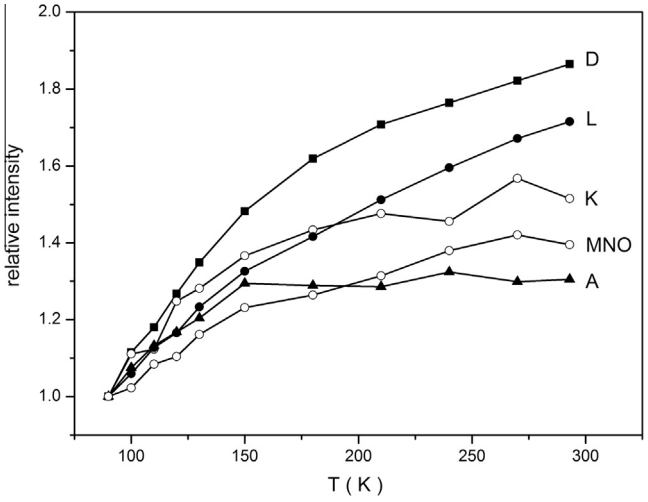

Fig. 3. Intensities of some α-polarized absorption bands relative to those at $T = 90$ K.

the main source of discrepancy between measured and calculated absorption band intensities.

When Ω_λ parameters are known, it is possible to find, with the help of Eq. (3), the strengths of transitions between excited states (see Table 4). Coefficients Γ^2_λ were taken from Ref. [32]. Probability of a spontaneous dipole transition between degenerate levels in a condensed matter is given by the relationship [42]

$$A_{IF} = \frac{64\pi^4 e^2 k_{IF}^3 n(k_{IF})}{3hg_I} s_{IF}. \quad (7)$$

Here g_I is the degeneracy of the initial multiplet, and $n(k_{IF})$ is the refractive index at the transition frequency. In order to find values of k_{IF} for transitions between excited states, our experimental data (Table 2) were used. The possibility of generating of stimulated emission for a specific emission channel is characterized by the multiplet luminescence branching ratio

$$\beta_{IF} = A_{IF} \Big/ \sum_F A_{IF} = A_{IF}\tau_I, \quad (8)$$

where τ_I is the excited state life time. The calculated values of the transition strengths, the spontaneous emission probabilities, the branching ratios of the transitions and lifetimes of the states are presented in Table 4. The largest branching ratios are preferably for transitions to the ground state. However, there are a number of transitions between excited states with substantial (>10%) branching ratios: $^4I_{11/2} \rightarrow {}^4I_{13/2}$; $^4I_{9/2} \rightarrow {}^4I_{13/2}$; $^4S_{3/2} \rightarrow {}^4I_{13/2}$; $^4F_{7/2} \rightarrow {}^4I_{13/2}$; $(^4F_{5/2} + {}^4F_{3/2}) \rightarrow {}^4I_{11/2}$, $^4I_{13/2}$; $^2G_{9/2} \rightarrow {}^4I_{13/2}$; $^4G_{11/2} \rightarrow {}^4I_{13/2}$; $(^4G_{9/2} + {}^2K_{15/2} + {}^2G_{7/2}) \rightarrow {}^4I_{11/2}$, $^4I_{13/2}$.

Luminescence spectra were recorded in the region of 536, 548, 662, 800, and 855 nm (see Figs. 4–9) with the excitation at 20490 cm^{-1} ($^4F_{7/2}$ state). The luminescence was measured at the normal incidence of the exciting light for the light emitted in the opposite direction. Therefore, both the exciting and emitted light had α-polarization for the sample cut perpendicular to C_3 axis of the crystal. π and σ-polarized spectra of some transitions (Figs. 7–9) were obtained on the sample with [110] orientation. Exciting light in the case of Figs. 7–9 had σ-polarization. The luminescence spectra at π-polarized excitation differ from those of Figs. 7–9 only in intensity, corresponding to value of the π-absorption on the wave length of the excitation. The same as in absorption, the luminescence is more intensive in σ-polarization. Shapes of the σ-polarized luminescence spectra coincide with those of the α-polarized spectra since observed transitions are of the electric dipole nature.

Majority of the emission spectra are easily identified (see Figure captions) according to transition energies from Figs. 1 and 2 and Table 4, except emission band at 800 nm (12500 cm^{-1}) shown in Fig. 6. Energy of this emission band corresponds to two transitions: $^4I_{9/2} \rightarrow {}^4I_{15/2}$ and $^2H_{11/2} \rightarrow {}^4I_{13/2}$ (Table 4). Additionally, these transitions have close emission probabilities (Table 4). However, real experimental emission intensity strongly depends on phonon relaxation and can substantially differ from the theoretical emission probability. Radiative probability of the excitation transfer $^4F_{7/2} \rightarrow {}^4I_{9/2}$ is much higher than that of $^4F_{7/2} \rightarrow {}^2H_{11/2}$ (Table 4). At the same time, conditions for phonon assisted excitation transfer are opposite, since $^2H_{11/2}$ state is much closer to $^4F_{7/2}$ state (Table 4). And at last, number of lines in the emission spectrum in the region of 12500 cm^{-1} (Fig. 6) is substantially larger than in the absorption spectrum (Fig. 1, σ-polarization) Thus, suggested identification of luminescence at 800 nm can take place.

The most intensive luminescence was observed at 548 nm (transition $^4S_{3/2} \leftrightarrow {}^4I_{15/2}$, Figs. 4 and 8). Number and positions of lines in the luminescence and absorption spectra of transitions $^4S_{3/2} \leftrightarrow {}^4I_{15/2}$ and $^2H_{11/2} \leftrightarrow {}^4I_{15/2}$ coincide (Fig. 4). Approximately similar correspondence takes place for $^4F_{9/2} \leftrightarrow {}^4I_{15/2}$ transitions (Figs. 5 and 1). This infers that both luminescence and absorption occur mainly with participation of the same crystal field levels of the ground and excited states. In absorption, the $^4I_{15/2} \rightarrow {}^2H_{11/2}$ transition is of ~16 times stronger than the $^4I_{15/2} \rightarrow {}^4S_{3/2}$ transition (Fig. 4 and Table 2), and the theoretical emission probability of $^2H_{11/2} \rightarrow {}^4I_{15/2}$ transition is of 5 times larger than that of $^4S_{3/2} \rightarrow {}^4I_{15/2}$ transition (Table 4), but in the observed luminescence correlation of intensities is opposite (Fig. 4), namely, integral luminescence intensity of the former band is 2.65 times smaller than that of the latter band.

In Ref. [12] in the impurity crystal $Er:YAl_3(BO_3)_4$ emissions from other excited manifolds besides $^4I_{13/2}$ were too weak to be detected. At the same time, in Ref. [43] a number of emission bands were observed in similar crystals. Emission due to $^4S_{3/2} \rightarrow {}^4I_{15/2}$ transition also was the most intensive one. In our case the crystal was excited into $^4F_{7/2}$ state. Radiative probability of the excitation transfer from $^4F_{7/2}$ to $^4S_{3/2}$ state is much smaller as compared with that to $^2H_{11/2}$ state (see Table 4). Therefore it is possible to suppose that the large emission intensity of $^4S_{3/2} \rightarrow {}^4I_{15/2}$ transition is due to effective phonon excitation transfer and not effective phonon relaxation. Additionally, there is also experimental contribution into the observed phenomenon. Absorption coefficient on wavelength 488 nm (20490 cm^{-1}) of the exciting radiation of argon laser is ~12 cm^{-1}. Corresponding penetration depth from the condition $\alpha x = 1$ is approximately 0.8 mm, while the sample thickness was 0.32 mm. Absorption coefficient of the smaller average value (~4 cm^{-1}) is in the region of the E absorption band (Fig. 4). Consequently, conditions for penetration of the exciting light and for the reverse propagation of the emitted light in the E-band are good enough. On the contrary, average absorption in the F-band is much larger

Table 4
Wave numbers (k_{IF}) and strengths (s_{IF}) of transitions, spontaneous emission probabilities (A), multiplet luminescence branching ratios (β) and life times of manifolds (τ).

Initial level	Final level	k_{IF} (cm^{-1})	s_{IF}, (10^{-20} cm^2)	A (s^{-1})	β (%)	τ (ms)
$^4I_{13/2}$ (Y)	$^4I_{15/2}$	6500	4.28	106.3	100	9.41
$^4I_{11/2}$(A)	$^4I_{13/2}$	3690	3.542	18.78	12.2	6.49
	$^4I_{15/2}$	10190	1.213	135.4	87.8	
$^4I_{9/2}$(B)	$^4I_{11/2}$	2210	0.5281	0.7218	0.44	6.15
	$^4I_{13/2}$	5900	1.976	51.39	31.58	
	$^4I_{15/2}$	12400	0.458	110.6	67.97	
$^4F_{9/2}$(D)	$^4I_{9/2}$	2780	0.714	1.942	0.15	0.80
	$^4I_{11/2}$	4990	3.863	60.78	4.84	
	$^4I_{13/2}$	8680	0.6251	51.76	4.12	
	$^4I_{15/2}$	15180	2.59	1140.4	90.88	
$^4S_{3/2}$(E)	$^4F_{9/2}$	3040	0.0725	0.6448	⩽0.1	0.58
	$^4I_{9/2}$	5820	0.8876	55.39	3.2	
	$^4I_{11/2}$	8030	0.2115	34.67	2.0	
	$^4I_{13/2}$	11720	0.9417	479.9	27.8	
	$^4I_{15/2}$	18220	0.601	1151	66.9	
$^2H_{11/2}$ (F)	$^4S_{3/2}$	900	0.5225	0.0402	⩽0.1	0.169
	$^4F_{9/2}$	3940	1.8291	11.80	0.2	
	$^4I_{9/2}$	6720	1.9537	62.56	1.1	
	$^4I_{11/2}$	8930	0.6189	46.51	0.8	
	$^4I_{13/2}$	12620	0.4075	86.42	1.5	
	$^4I_{15/2}$	19120	4.748	5715	96.4	
$^4F_{7/2}$ (G)	$^2H_{11/2}$	1330	1.7292	0.6439	⩽0.1	0.288
	$^4S_{3/2}$	2230	0.0149	0.02615	⩽0.1	
	$^4F_{9/2}$	5270	0.1852	4.290	⩽0.1	
	$^4I_{9/2}$	8050	1.4803	122.2	3.5	
	$^4I_{11/2}$	10260	1.0885	186.1	5.4	
	$^4I_{13/2}$	13950	0.8396	360.8	10.4	
	$^4I_{15/2}$	20450	2.068	2799	80.6	
$F_{5/2}$ + $^4F_{3/2}$ (H + I)	$^4F_{7/2}$	1750	0.9329	0.6331	⩽0.1	0.376
	$^2H_{11/2}$	3080	0.6517	2.411	⩽0.1	
	$^4S_{3/2}$	3980	0.1765	1.409	⩽0.1	
	$^4F_{9/2}$	7020	1.747	76.53	2.9	
	$^4I_{9/2}$	9800	1.197	142.65	5.4	
	$^4I_{11/2}$	12010	1.80	394.8	14.8	
	$^4I_{13/2}$	15700	1.47	720.3	27.1	
	$^4I_{15/2}$	22200	0.953	1320.3	49.7	
$^2G_{9/2}$ (K)	$^4F_{3/2}$ + $^4F_{5/2}$	2330	0.2175	0.3484	⩽0.1	0.335
	$^4F_{7/2}$	4080	0.702	6.037	0.2	
	$^2H_{11/2}$	5410	0.7877	15.79	0.5	
	$^4S_{3/2}$	6310	0.0115	0.3659	⩽0.1	
	$^4F_{9/2}$	9350	0.2053	21.25	0.7	
	$^4I_{9/2}$	12130	0.0987	223.0	7.5	
	$^4I_{11/2}$	14340	0.7204	268.99	9.1	
	$^4I_{13/2}$	18030	1.639	1216.4	40.7	
	$^4I_{15/2}$	24530	0.66	1233.5	41.1	
$^4G_{11/2}$ (L)	$^2G_{9/2}$	1870	2.0678	1.427	⩽0.1	0.072
	$^4F_{3/2}$ + $^4F_{5/2}$	4200	0.6251	4.887	⩽0.1	
	$^4F_{7/2}$	5950	0.7908	17.58	0.13	
	$^2H_{11/2}$	7280	0.5195	21.15	0.15	
	$^4S_{3/2}$	8180	0.3362	19.42	0.14	
	$^4F_{9/2}$	11220	2.1955	327.2	2.34	
	$^4I_{9/2}$	14000	0.4452	128.90	0.92	
	$^4I_{11/2}$	16210	0.1614	72.54	0.52	
	$^4I_{13/2}$	19900	1.859	1545.8	11.1	
	$^4I_{15/2}$	26400	6.10	11843	84.7	
$^4G_{9/2}$ + $^2K_{15/2}$ + $^2G_{7/2}$ (M, N, O)	$^4G_{11/2}$	1150	3.67	0.2079	⩽0.1	0.183
	$^2G_{9/2}$	3020	2.367	2.428	⩽0.1	
	$^4F_{3/2}$ + $^4F_{5/2}$	5350	4.309	24.57	0.44	
	$^4F_{7/2}$	7100	4.041	53.86	0.98	
	$^2H_{11/2}$	8430	5.742	128.11	2.3	
	$^4S_{3/2}$	9330	1.061	32.09	0.6	
	$^4F_{9/2}$	12370	3.156	222.5	4.1	
	$^4I_{9/2}$	15150	3.138	406.4	7.4	
	$^4I_{11/2}$	17360	5.296	1032	18.9	
	$^4I_{13/2}$	21050	6.644	2308	42.2	
	$^4I_{15/2}$	27550	1.619	1261	23.0	

($\sim$40 cm^{-1}), and substantial part of the emitted light is absorbed on the reverse path to the sample surface, with subsequent reemission into 4π angle. Thus, concentration quenching of luminescence is not very important for $^4S_{3/2} \rightarrow {}^4I_{15/2}$ emission in conditions of the present experiment.

4. Summary

Single crystal of $ErAl_3(BO_3)_4$ was grown and its structure was studied. Polarized absorption spectra of $ErAl_3(BO_3)_4$ single crystal were measured in the spectral range 1670–330 nm

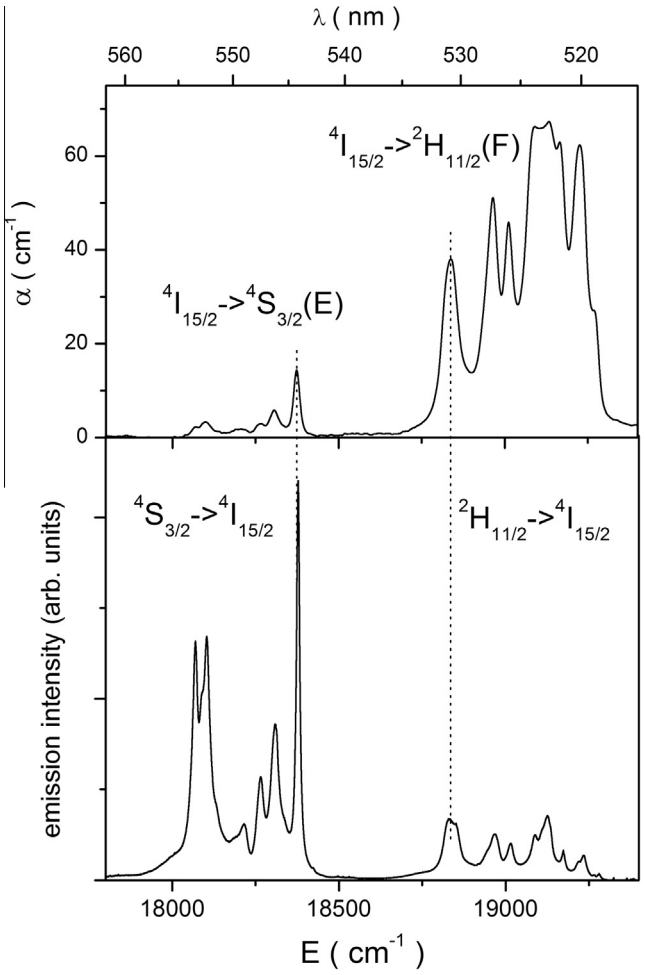

Fig. 4. α-polarized absorption and emission spectra of transitions ${}^4I_{15/2} \leftrightarrow {}^4S_{3/2}$ and ${}^4I_{15/2} \leftrightarrow {}^2H_{11/2}$ at room temperature.

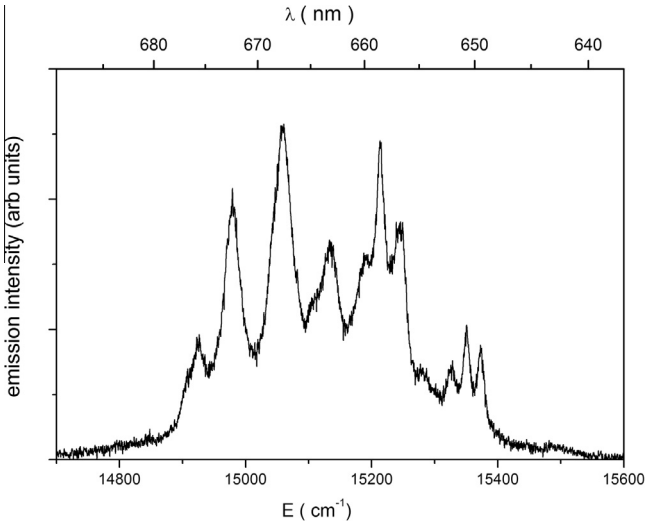

Fig. 5. α-polarized emission spectrum of ${}^4F_{9/2} \rightarrow {}^4I_{15/2}$ transition at room temperature.

(6000–30000 cm^{-1}). The Judd–Ofelt parameters at room temperature have been determined as: $\Omega_2 = 4.87 \cdot 10^{-20}\ cm^2$, $\Omega_4 = 2.49 \cdot 10^{-20}\ cm^2$, $\Omega_6 = 2.72 \cdot 10^{-20}\ cm^2$. The parameters have

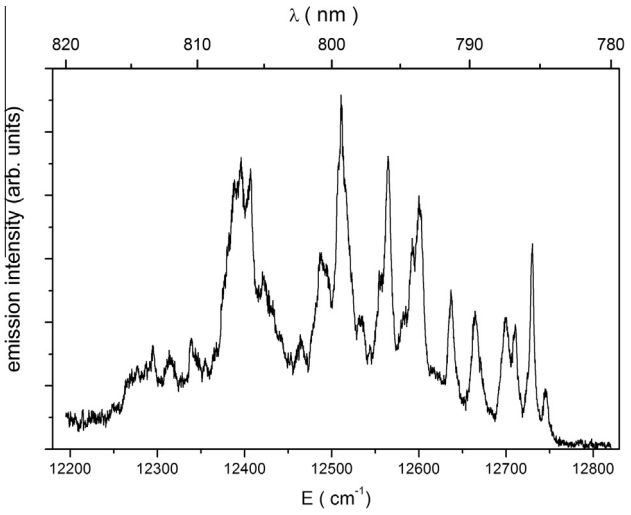

Fig. 6. α-polarized emission spectrum of ${}^2H_{11/2} \rightarrow {}^4I_{13/2}$ and ${}^4I_{9/2} \rightarrow {}^4I_{15/2}$ transitions at room temperature.

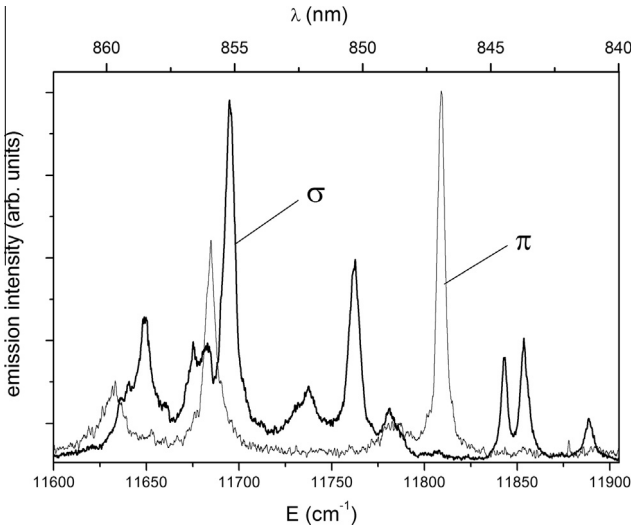

Fig. 7. π and σ-polarized emission spectra of ${}^4S_{3/2} \rightarrow {}^4I_{13/2}$ transition at room temperature.

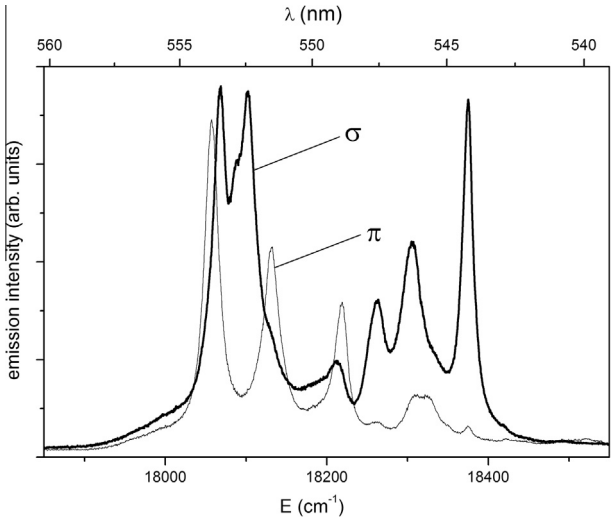

Fig. 8. π and σ-polarized emission spectra of ${}^4S_{3/2} \rightarrow {}^4I_{15/2}$ transition at room temperature.

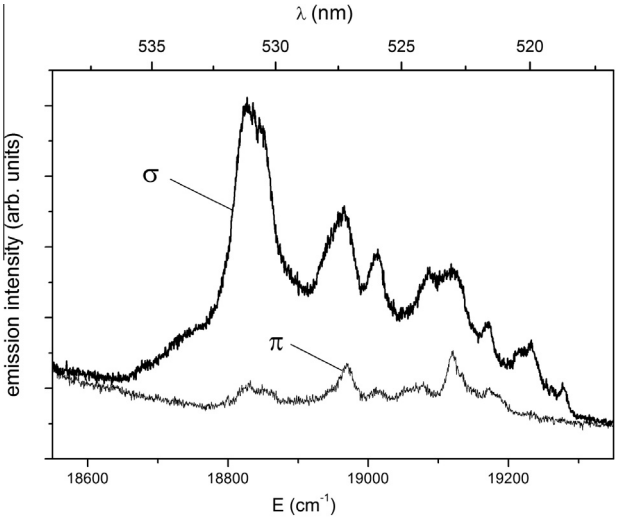

Fig. 9. π and σ-polarized emission spectra of $^2H_{11/2} \rightarrow {}^4I_{15/2}$ transition at room temperature.

been used to calculate the spontaneous emission probabilities, the multiplet luminescence branching ratios and the fluorescence life times of the manifolds. The absorption band intensities substantially and differently change with the temperature. Consequently, the J–O parameters also depend on temperature. Different dependence of the intensities on temperature results in additional error in determination of the J–O parameters. The luminescence spectra due to transitions $^2H_{11/2} \rightarrow {}^4I_{15/2}$ (526 nm), $^4S_{3/2} \rightarrow {}^4I_{15/2}$ (548 nm), $^4F_{9/2} \rightarrow {}^4I_{15/2}$ (662 nm), $^2H_{11/2} \rightarrow {}^4I_{13/2} + {}^4I_{9/2} \rightarrow {}^4I_{15/2}$ (800 nm) and $^4S_{3/2} \rightarrow {}^4I_{13/2}$ (855 nm) were recorded in α, σ and π polarizations. The most intensive luminescence in the $ErAl_3(BO_3)_4$ single crystal was observed at 548 nm ($^4S_{3/2} \rightarrow {}^4I_{15/2}$ transition).

Acknowledgements

The work was supported by the Russian Foundation for Basic Researches grant 12-02-00026, by the Russian President Grants SS-1044.2012.2 and 4828.2012.2, by project *No* 3.9.5 PSB RAS, and by the Ministry of Education and Science of Russian Federation grant 8365.

References

[1] Y.J. Chen, Y.F. Lin, X.H. Gong, Q.G. Tan, Z.D. Luo, Y.D. Huang, Appl. Phys. Lett. 89 (2006) 241111.
[2] N.I. Leonyuk, V.V. Maltsev, E.A. Volkova, O.V. Pilipenko, E.V. Koporulina, V.E. Kisel, N.A. Tolstik, S.V. Kurilchik, N.V. Kuleshov, Opt. Mater. 30 (2007) 161.
[3] Y. Chen, Y. Lin, X. Gong, J. Huang, Z. Luo, Y. Huang, Opt. Lett. 37 (2012) 1565.
[4] A.A. Kaminskii, V.S. Mironov, A. Kornienko, S.N. Bagaev, G. Boulon, A. Brenier, B. Di Bartolo, Phys. Status Solidi (a) 151 (1995) 231.
[5] J. Amin, B. Dussardier, T. Scweizer, M. Hempstead, J. Lumin. 69 (1996) 17.
[6] J.A. Capobianco, P. Kabro, F.S. Ermeneux, R. Moncorge, M. Bettinelli, E. Cavalli, Chem. Phys. 214 (1997) 329.
[7] D.K. Sardar, W.M. Bradley, J.J. Perez, J.B. Gruber, B. Zandi, J.A. Hutchinson, C.W. Trussell, M.R. Kokta, J. Appl. Phys. 93 (2003) 2602.
[8] Q. Wang, N.K. Dutta, R. Ahrens, J. Appl. Phys. 95 (2004) 4025.
[9] A. Baraldi, R. Capelletti, N. Magnani, M. Mazzera, E. Beregi, I. Földvári, J. Phys.: Condens. Matter 17 (2005) 6245.
[10] M. Dammak, J. Alloys Compd. 393 (2005) 51.
[11] I. Földvári, E. Beregi, R. Capelletti, A. Baraldi, Phys. Status Solidi (c) 2 (2005) 260.
[12] W. You, Y. Lin, Y. Chen, Z. Luo, Y. Huang, Opt. Mater. 29 (2007) 488.
[13] W. You, Y. Huang, Y. Chen, Y. Lin, Z. Luo, Phys. B 405 (2010) 34.
[14] P. Dekker, J.M. Dawes, J.A. Piper, Y.G. Liu, J.Y. Wang, Opt. Commun. 195 (2001) 431.
[15] E. Cavalli, A. Speghini, M. Bettinelli, M.O. Ramirez, J.J. Romero, L.E. Bausa, J.G. Sole, J. Lumin. 102 (2003) 216.
[16] M. Rico, M.C. Pujol, F. Díaz, C. Zaldo, Appl. Phys. B 72 (2001) 157.
[17] R.A. McFarlane, Appl. Phys. Lett. 54 (1989) 2301.
[18] J.Y. Allain, M. Monerie, H. Poignant, Electron. Lett. 28 (1992) 111.
[19] D. Jaque, O. Enguita, U. Caldino, M.O. Ramirez, J. Garcia, J. Appl. Phys. 90 (2001) 561.
[20] M. Montes, D. Jaque, Z.D. Luo, Y.D. Huang, Opt. Lett. 30 (2005) 397.
[21] Z. Huang, X. Gong, Y. Huang, Z. Luo, Opt. Commun. 237 (2004) 389.
[22] I.A. Gudim, E.V. Eremin, V.L. Temerov, J. Cryst. Growth 312 (2010) 2427.
[23] K. Teshima, Y. Kikuchi, T. Suzuki, S. Oishi, Cryst. Growth Des. 6 (2006) 1766.
[24] K.N. Boldyrev, M.N. Popova, M. Bettinelli, V.L. Temerov, I.A. Gudim, L.N. Bezmaternykh, P. Loiseau, G. Aka, N.I. Leonyuk, Opt. Mater. 34 (2012) 1885.
[25] D. Neogy, K.N. Chattopadhyay, P.K. Chakrabarti, H. Sen, B.M. Wanklyn, J. Phys. Chem. Solids 59 (1998) 783.
[26] H.D. Flack, Acta Crystallogr. A39 (1983) 876.
[27] G.M. Sheldrick, Acta Crystallogr. A64 (2008) 112.
[28] G.M. Sheldrick, Shelx-97: A Computer Program for Refinement of Crystal Structures, University of Göttingen, Germany, 1997.
[29] N.I. Leonyuk, L.I. Leonyuk, Prog. Cryst. Growth Charact. Mater. 31 (1995) 179.
[30] I. Couwenberg, K. Binnemans, H. De Leebeeck, C. Görller-Walrand, J. Alloys Compd. 274 (1998) 157.
[31] A.S. Aleksandrovsky, A.V. Malakhovskii, A.S. Krylov, V.N. Voronov, J. Lumin. 132 (2012) 690.
[32] A.A. Kaminskii, Crystalline Lasers: Physical processes and Operating Schemes, CRC Press, New York, London, Tokyo, 1996.
[33] A.V. Malakhovskii, A.E. Sokolov, V.L. Temerov, L.N. Bezmaternykh, A.L. Sukhachev, V.A. Seredkin, S.L. Gnatchenko, I.S. Kachur, V.G. Piryatinskaya, Fiz. Tverd. Tela 50 (2008) 1237 (Phys. Solid State 50 (2008) 1287).
[34] G.H. Jia, C.Y. Tu, J.F. Li, Z.J. Zhu, Z.Y. You, Y. Wang, B.C. Wu, J. Appl. Phys. 96 (2004) 6262.
[35] R. Vázquez, R. Osellame, M. Marangoni, R. Ramponi, E. Diéguez, Opt. Mater. 26 (2004) 231.
[36] I.I. Sobel'man, Introduction to the Theory of Atomic Spectra, Oxford, Pergamon, 1972 (Nauka, Moscow, 1977).
[37] B.R. Judd, Phys. Rev. 127 (1962) 750.
[38] G.S. Ofelt, J. Chem. Phys. 37 (1962) 511.
[39] R.D. Peacock, Struct. Bond. 22 (1975) 83.
[40] W.F. Krupke, IEEE J. Quantum. Electron. QE-7 (1971) 153.
[41] H. Jiang, J. Wang, X. Hu, H. Liu, X.Y. Liu, Chem. Phys. Lett. 365 (2002) 279.
[42] V.L. Ginzburg, Theoretical Physics and Astrophysics, Nauka, Moscow, 1975 (Pergamon, Oxford, 1979).
[43] I. Földvári, E. Beregi, P. Solarz, G. Dominiak-Dzik, W. Ryba-Romanovski, A. Watterich, Phys. Status Solidi (c) 4 (2007) 893.